Bubble induced mixing in a bubble column with counter-current liquid flow

P. Kováts[1,*], K. Zähringer[1],
1: Laboratory of Fluid Dynamics and Technical Flows, Otto-von-Guericke-Universität Magdeburg, Germany
*Correspondent author: peter.kovats@ovgu.de
Keywords: Mixing, LIF, Two-phase flow, Counter-current flow, Sulforhodamine G

ABSTRACT

Bubble columns have been widely investigated over the last few decades, concentrating on the bubble parameters, and gas/liquid motion. However, mixing and often the resulting interaction between chemical reaction and hydrodynamics in the column are rarely analysed. For this reason, experiments with Laser Induced Fluorescence (LIF) applying Sulforhodamine G as fluorescent dye, and shadow imaging were performed in a square laboratory-scale counter-current flow bubble column at 21 different flow conditions and three different dye inlet positions. In these experiments the mixing efficiency was investigated by varying the bubble size, the gas and the liquid flow rates, to obtain the necessary data for a further understanding of mixing processes in bubbly flows. The strong influence of the bubble presence, their size and the counter-current liquid flow rate on mixing in the column is obvious from these results. Bubble induced mixing leads to a good homogenisation inside the column, compared to a flow without bubbles. Also, the larger the bubbles the higher the bubble induced upward velocity, which leads to a better mixing. The highest counter-current liquid flow rate led to a more concentrated dye jet, which was less dispersed than at lower liquid flow rates, while the moderate counter-current liquid flow rate (11.1 l· min-1) has been found optimal for mixing in the investigated cases. The combination of large bubbles generated with the 3.6 mm capillaries, and a moderate counter-current liquid flow rate led to the best mixing performance in the bubble column.

1. Introduction

Mixing in a bubble column and the resulting interaction between chemical reaction and hydrodynamics in the column is an important process step for reactions with moderate speed taking place in that column. In this case, a significant reciprocal influence between mixing and the reaction within the bubble column is to be expected. Further, bubble induced flow mixing itself is subject of continuous research efforts, but unfortunately, experimental investigations of the reciprocal influence of mixing and reactive mass transfer for less rapid reactions in multiphase reaction apparatuses can rarely be found in the literature.

The mixing caused by a bubble swarm and the associated concentration fluctuations in a rectangular bubble column, as well as the mass transfer of individual bubbles, were analysed by a group at the IMFT in Toulouse [Alméras et al., 2016; Bouche et al., 2013; Roudet et al., 2017]. This group of authors also analysed the mixing effects in a pseudo-2d bubble column [Alméras et al., 2018]. Studies of the mixing behaviour of bubble columns using Euler-Euler simulations

can also be found sporadically in the literature [Wiemann et al., 2005; Bai et al., 2012; Bothe et al., 2007; Ekambara et al., 2003]. Usually, mixing in bubble columns is characterised in the literature by the axial dispersion model, but the dependencies on different operational parameters are often neglected: dependency on the bubble size [Shetty et al., 1992], gas and possibly liquid flow rate or the column geometry, have so far only been dealt with incompletely.
For this reason, in the present study an extensive experimental measurement campaign has been undertaken to obtain the necessary data for a further understanding of mixing processes in bubbly flows. Different gas inlet configurations are used to investigate the influence of the bubble size and the distribution of the bubbles by varying the gas and liquid flow rates in the counter-current model bubble column.

2. Experimental set-up

The combined laser-induced fluorescence (LIF) and shadow imaging measurements have been executed in a square laboratory-scale bubble column made of acrylic glass with an inner side length of d=0.100 m and a height of h=2 m (Figure. 1, #1). A bubble curtain was generated 500 mm from the bottom of the column with 7 capillaries placed in line in the centre of the bubble column (Figure. 1, #3) and bubbles in a size range of 1 to 9 mm are produced by introducing air through different diameter capillaries (0.13, 0.18 and 3.6 mm). Gas flow rates of 10 $l \cdot h^{-1}$ and 48 $l \cdot h^{-1}$ were investigated in stagnant liquid and at four different counter-current liquid flow conditions. The images have been recorded with four 5 Mpixel sCMOS PIV-cameras (LaVision Imager sCMOS) (Figure. 1, #2) equipped with 50 mm Nikon Micro lenses and appropriate longpass filters to simultaneously record the emitted light of the injected fluorescent dye Sulforhodamine G over the entire measurement section (1 m) of the column (Figure. 1, #4). The cameras were focused to the laser light sheet generated by a Nd:YAG double pulse laser (Evergreen PIV, 532 nm) in the centre of the column. Through a stainless steel capillary Sulforhodamine G fluorescent dye with a concentration of c_{max} = 0.1 $mg \cdot l^{-1}$ and 10 $ml \cdot min^{-1}$ flow rate was introduced with a syringe pump into the flow at three different heights (250 mm, 500 mm and 750 mm) in the centre plane of the column. To be able to mask the bubble shadows from the LIF images, additionally, eight high-power LEDs were used together with a sheet of thin drawing paper, as light diffusor, on the back wall of the column to obtain homogeneous light distribution for the shadow images of the bubbles. These were acquired on the second frame of the cameras and triggered with an interframe time of 40 μs to the LIF images, which assured that bubbles did not move noticeably in-between both frames. This second frame allows to mask the

bubble shadows during LIF image processing and to obtain simultaneously the bubble size distribution of the specific measurement condition.

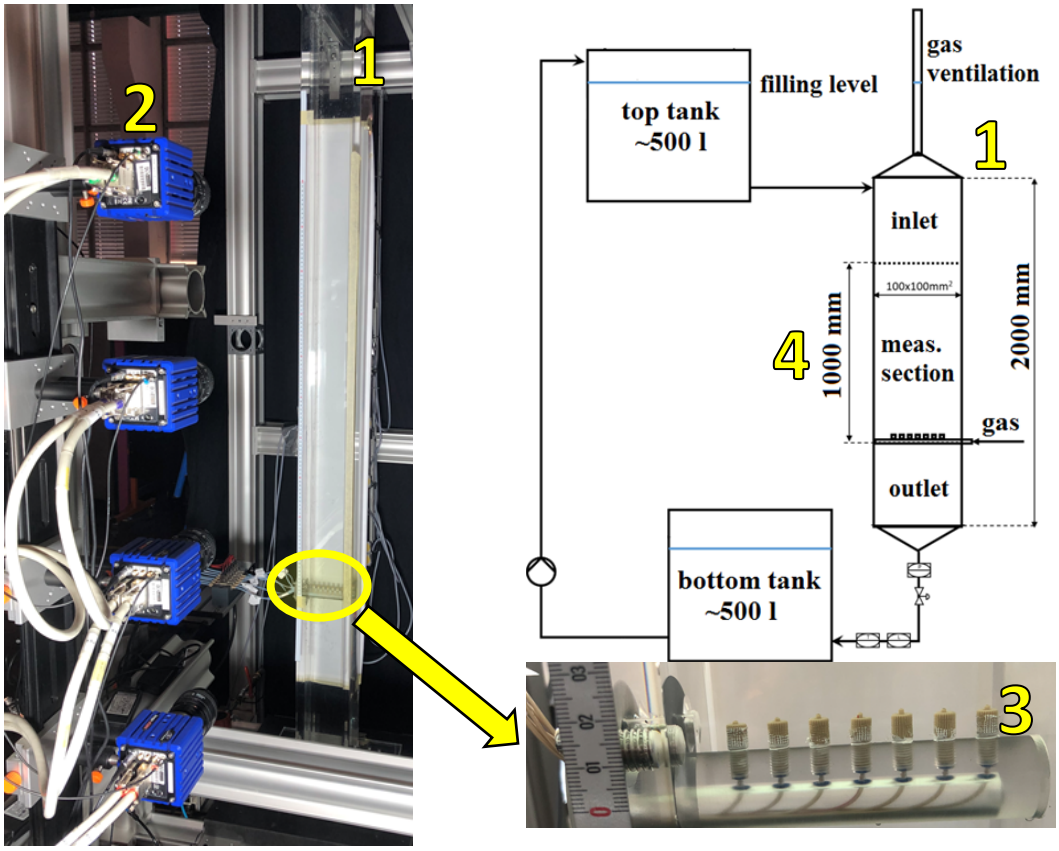

Figure. 1 Experimental setup.

Table. 1 Investigated cases.

Capillary inner diameter/ material	Gas	Superficial gas velocity [m· s^{-1}]	Gas flow rate [l· h^{-1}]	Superficial liquid velocity [m· s^{-1}]	Counter-current liquid flow rate [l· min^{-1}]	Column Reynolds number $\left(Re = \frac{d \cdot v_{Ls} \cdot \rho_L}{\mu_L}\right)$
0.13 mm/ stainless steel	Air	2.8· 10^{-4}	10	0 1· 10^{-3} 5.2· 10^{-3} 1.9· 10^{-2} 9.3· 10^{-2}	0 0.6 3.1 11.1 55.5	0 100 500 1800 9000
0.18 mm/ Teflon	Air	2.8· 10^{-4}	10	0 1· 10^{-3} 5.2· 10^{-3} 1.9· 10^{-2} 9.3· 10^{-2}	0 0.6 3.1 11.1 55.5	0 100 500 1800 9000
3.6 mm/ PEEK	Air	2.7· 10^{-4} 1.3· 10^{-3}	9.7 48.4	0 1· 10^{-3} 5.2· 10^{-3} 1.9· 10^{-2} 9.3· 10^{-2}	0 0.6 3.1 11.1 55.5	0 100 500 1800 9000

The geometrical calibration was performed in the whole measurement area with a half meter long 3D calibration plate. With this experimental setup 3x1500 pictures were taken with 5 Hz recording rate for each investigated operational case. The investigated flow conditions are listed in Table 1.

3. Data processing

The recorded images were processed in DaVis 8.4 (LaVision). The first step was to mask the bubbles from the LIF images (first frame of each image pair). To this end, a mask was created from the bubble shadow images (second frame of each image pair) and was applied to the LIF images (Figure 2.).

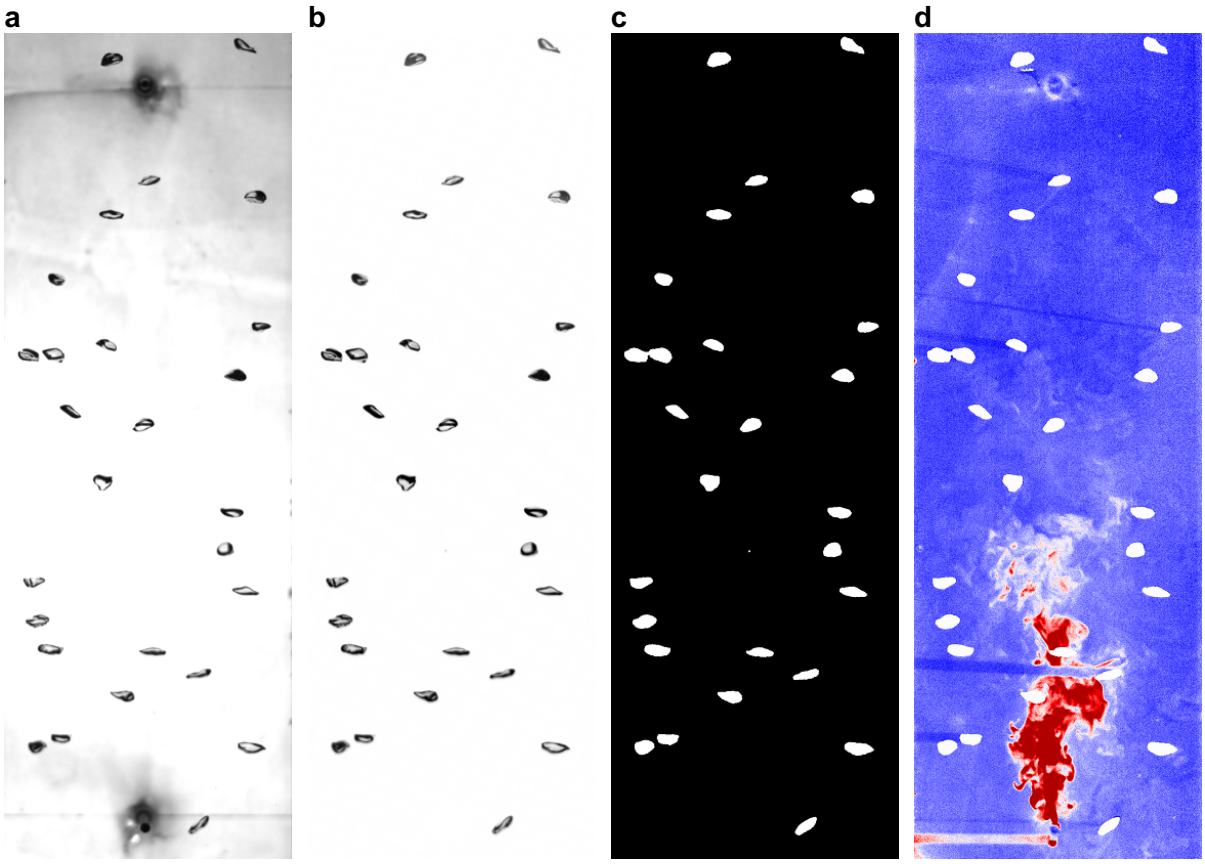

Figure. 2 Image processing: raw shadow image (a), image with subtracted background (b), binarized mask (c) mask applied to the LIF image (d).

In the next step, the fluorescence intensity of the masked LIF images was converted into concentrations with the help of a linear calibration curve for different Sulforhodamine G concentrations (example in Figure 3). Preliminary investigations have shown, that the emitted

fluorescence intensity is linear to the dye concentration in the investigated concentration and laser energy ranges.

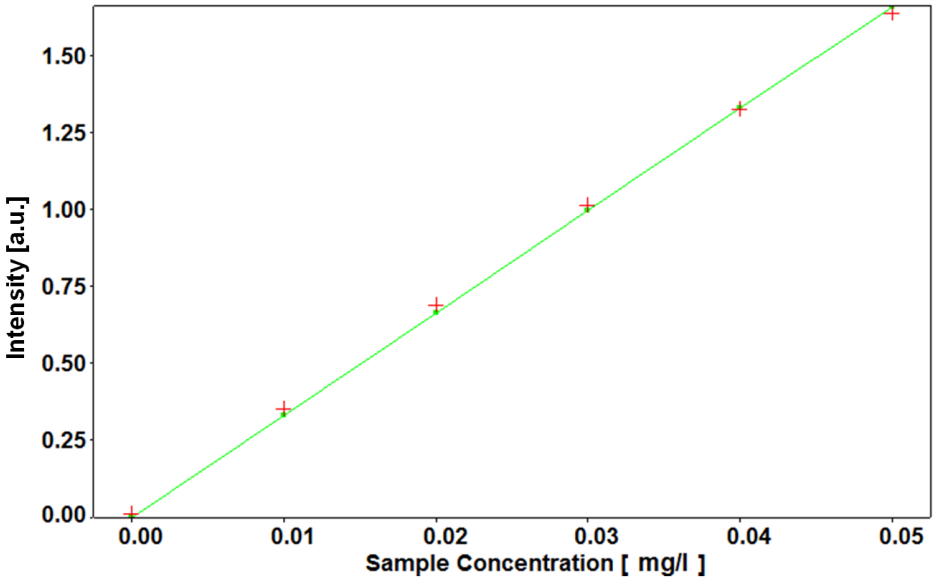

Figure. 3 Concentration calibration curve of Sulforhodamine G.

After these image processing steps, the images of the four cameras were stitched together to be able to track in time the concentration change over the whole column height.

4. Quantification of mixing intensity

Figure 4 shows some exemplary snapshots from the measurements with 0.13 mm capillaries in stagnant liquid (left two images) and at 11.1 l· min^{-1} counter-current liquid flow rate (right two images). It is clearly visible by comparing the left and right images of each pair (a-b; c-d) without and with bubbles respectively, that the bubbles destroy the fluorescent dye jet by an increased mixing with the surrounding liquid.

Compared to the stagnant case (Figure 4 a), the counter-current liquid flow (Figure 4 c) pushes the dye jet downwards. Nevertheless, the two snapshots with bubbly flow look very similar, since the bubbles entrain the liquid upwards and enhances mixing.

In order to quantify the mixing achieved in the column the concentration data presented in Figure 4 has been treated further.

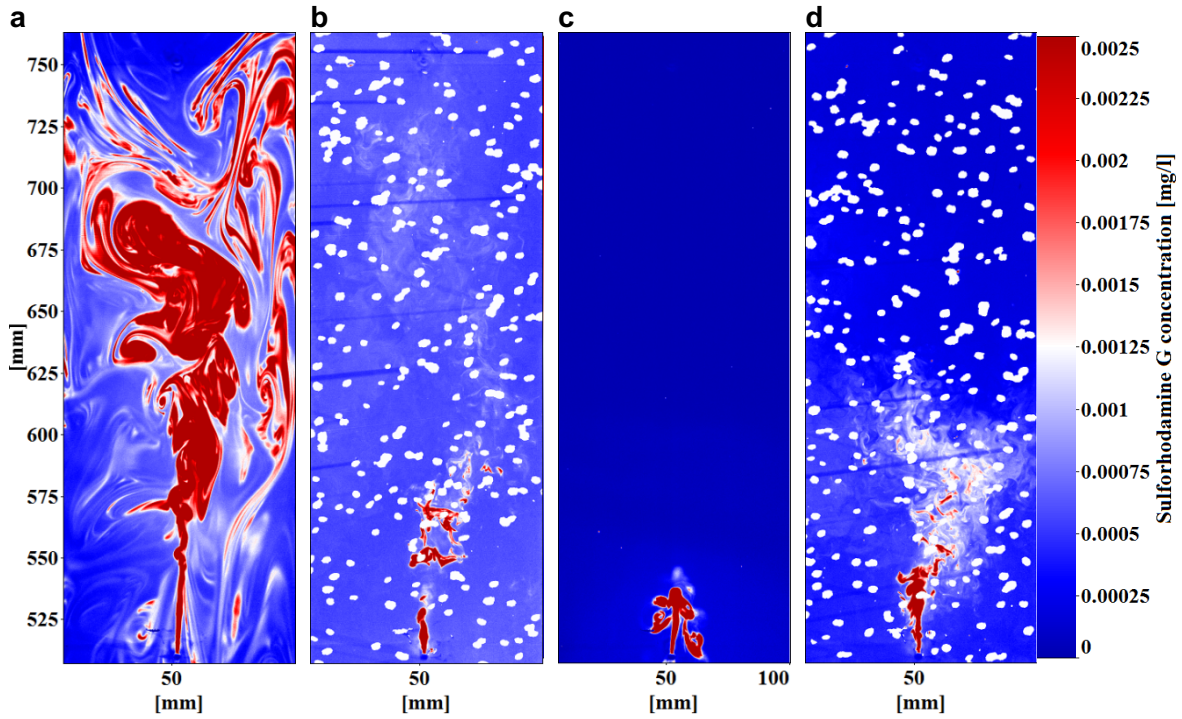

Figure. 4 Exemplary snapshots from the third camera (500-760 mm) without (a) and with (b) bubbles in stagnant liquid, and without (c) and with (d) bubbles at 11.1 l· min^{-1} counter-current liquid flow rate. Dye inlet at 500 mm, bubbles generated with 0.13 mm capillaries, t=200 seconds from dye start.

First of all, theoretical dye concentrations for perfect mixing were calculated for every investigated counter-current liquid flow rate and time step after first dye injection (Figure. 5). Evidently, the concentration for perfect mixing increases with time, since more and more dye is injected. In contrary, with increasing counter-current liquid flow rate, the dye accumulation in the column decreases, because increasing amount of dye is washed out. These theoretical values apply for all three dye injection points.

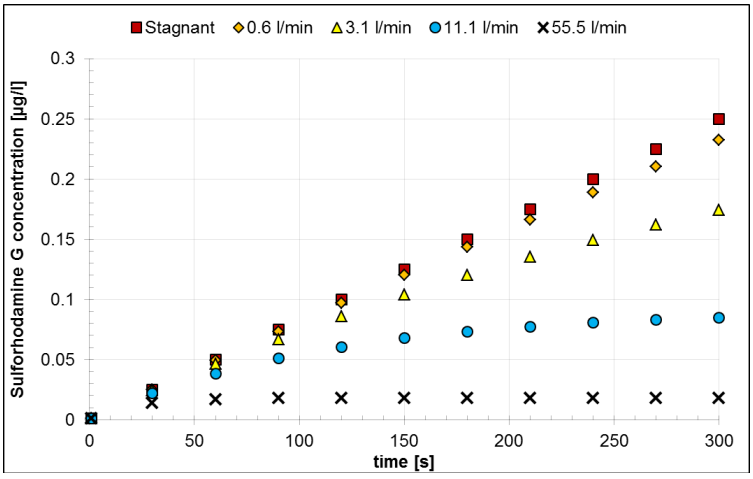

Figure. 5 Theoretical perfect mixing dye concentrations at different counter-current liquid flow rates.

Then, a mixing coefficient has been defined according to common mixing definitions, e.g. [Kováts et al., 2020]. For this, both - the theoretical and measured concentrations - were normalized with the injected maximum concentration according to Eq. 1.:

$$c_n = \frac{c - c_{min}}{c_{max} - c_{min}} \quad (1)$$

where c_{max} is the injected dye concentration and c_{min} corresponds to a minimum background concentration, which is zero for perfect mixing, while for the experiments it is equal to the equivalent concentration of the first recorded image for each run, when no dye is in the system, and therefore it is close to zero.

Figure. 6 shows the result of this normalization for an exemplary case, where the dye was introduced at 500 mm in a bubble swarm generated with 0.18 mm capillaries at 11.1 l· min^{-1} counter-current liquid flow rate. For this figure, the average dye concentrations in several vertical sections have been calculated over the column width in function of time and compared to the value for perfect mixing presented before and normalized in the same manner.

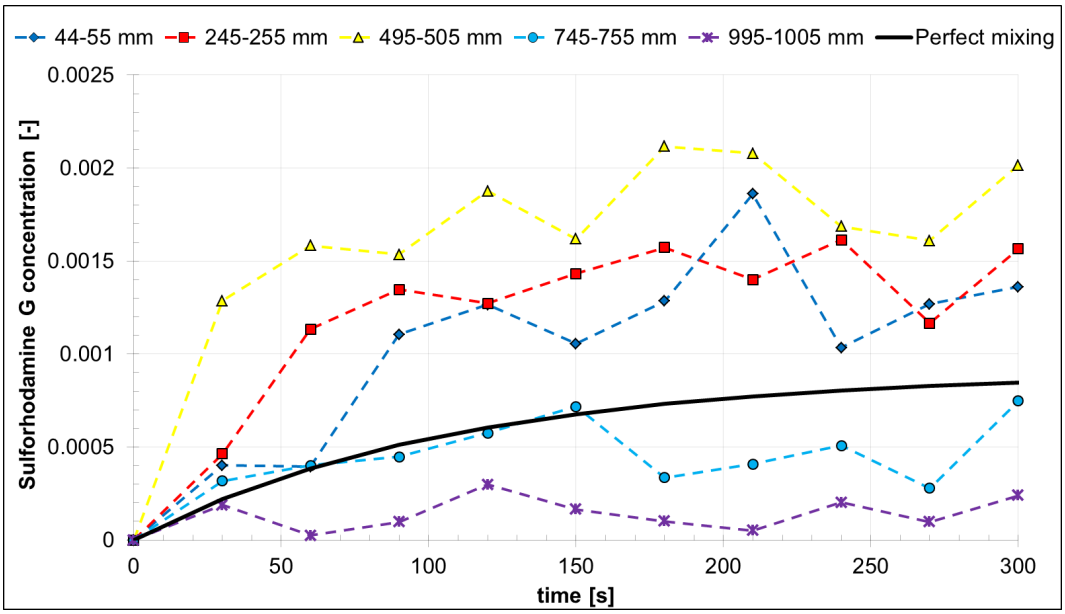

Figure. 6 Normalized theoretical and measured dye concentrations during 300 seconds of dye injection at 11.1 l· min^{-1} counter-current liquid flow rate at different heights. Dye inlet at 500 mm, bubbles generated with 0.18 mm capillaries.

The noticeably small values of the normalized concentration in Fig. 6 originate from the averaging process over the column width, where the dye is only present in the centre. Obviously, in the column sections below the inlet (<500 mm, blue, red and yellow marks) higher concentrations than the concentration for perfect mixing (black line) were measured, since the counter-current liquid flow transported most of the injected dye downwards. Appreciably less

dye is transported by the bubbles to the upper part of the bubble column (light blue and purple marks). Therefore, in the upper sections the normalized dye concentration is smaller than for perfect mixing. In these higher column regions after a while the concentration stays more or less constant, while it increases in the lower column sections.

For a further analysis, and comparison of the results from different counter-current liquid flow rates, the experimental normalized concentrations $c_{n,exp}$ have been divided by the normalized theoretical concentration for perfect mixing $c_{n,theor}$ of the respective counter-current liquid flow rate.

$$c_{norm} = \frac{c_{n,exp}}{c_{n,theor}} \qquad (2)$$

Figure. 7 shows these normalized concentrations for the exemplary case from Figure. 6. In the bottom part of the column (blue, red and yellow marks) the injected dye is dispersed more and more in the column and the normalized dye concentration ratios get closer to perfect mixing with the value one (black line). In the upper part of the column, where less dye is transported due to the counter-current liquid flow, the dye concentration ratios are smaller than the value for perfect mixing $c_{norm} = 1$.

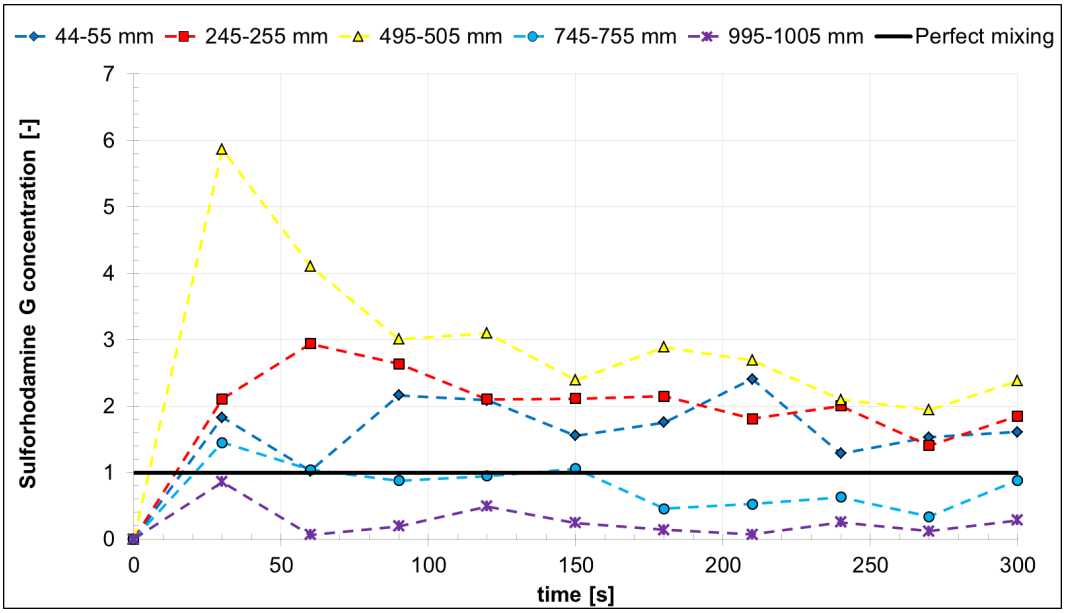

Figure. 7 Normalized dye concentration ratios measured during 300 seconds of dye injection at 11.1 l· min^{-1} counter-current liquid flow rate for different heights. Dye inlet at 500 mm, bubbles generated with 0.18 mm capillaries.

5. Results

To compare the mixing efficiency for different investigated cases the normalized dye concentration ratios at 300 s after injection start will be used in the following discussion.

Corresponding to industrial processes, the results in this section are discussed according to batch (stagnant cases), and continuous (with counter-current liquid flow) processes.

5.1. Stagnant cases

In stagnant liquid cases, the column was filled with water and the dye was introduced through the capillary at different heights into the column.

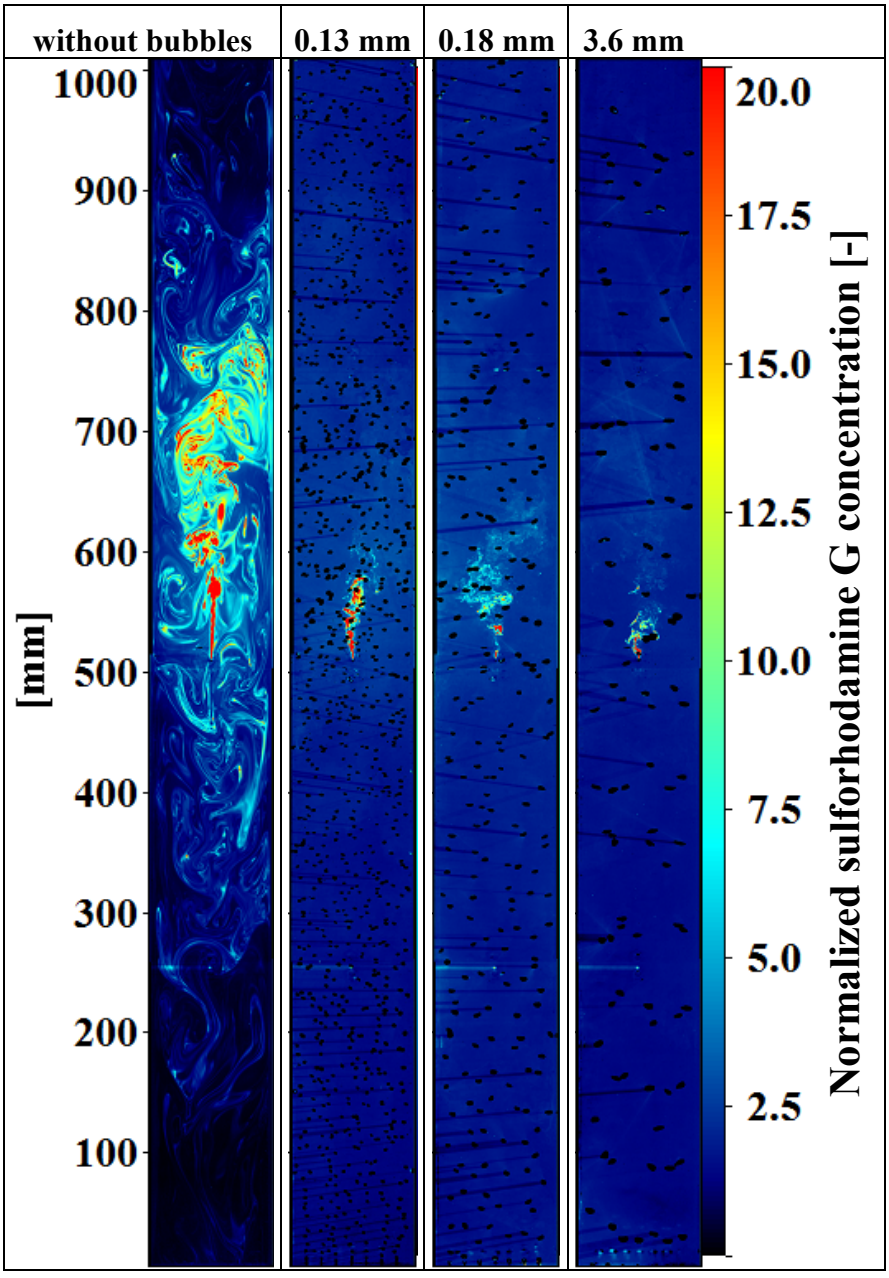

Figure. 8 Snapshots of the experiments for stagnant water at t=300 s with and without bubbles. Dye inlet at 500 mm, bubbles generated with 0.13, 0.18 and 3.6 mm capillaries.

Figure. 8 shows some exemplary snapshots of the normalized concentrations 300 s after the start of dye injection. In the case without bubbles mixing occurs due to the jet of the dye inlet. For this reason, undisturbed, large scale dye structures can be found and the concentration ratios are far from perfect mixing with a value of one.

By introducing bubbles, the large dye structures vanish and the bubble induced liquid flow enhances mixing. The measured concentration distributions are similar for all three bubble sizes, except in the area just above to the dye inlet.

Figure. 9 shows the normalized concentration ratios at t=300 s for all investigated cases in function of the column height and for the three dye injection heights.

In the stagnant case without bubbles (top diagram of Figure 9), the highest concentration can be observed around the injection height. With increasing capillary diameter, and thus increasing bubble size, the dye concentration peak decreases due to the stronger vertical liquid motion induced by the bigger bubbles. The stronger upward liquid flow and liquid recirculation in the column leads to a better mixing at larger bubble size. From the investigated cases the best mixing performance is reached with the largest capillary (3.6 mm) and at the highest gas flow rate (50 $l \cdot min^{-1}$).

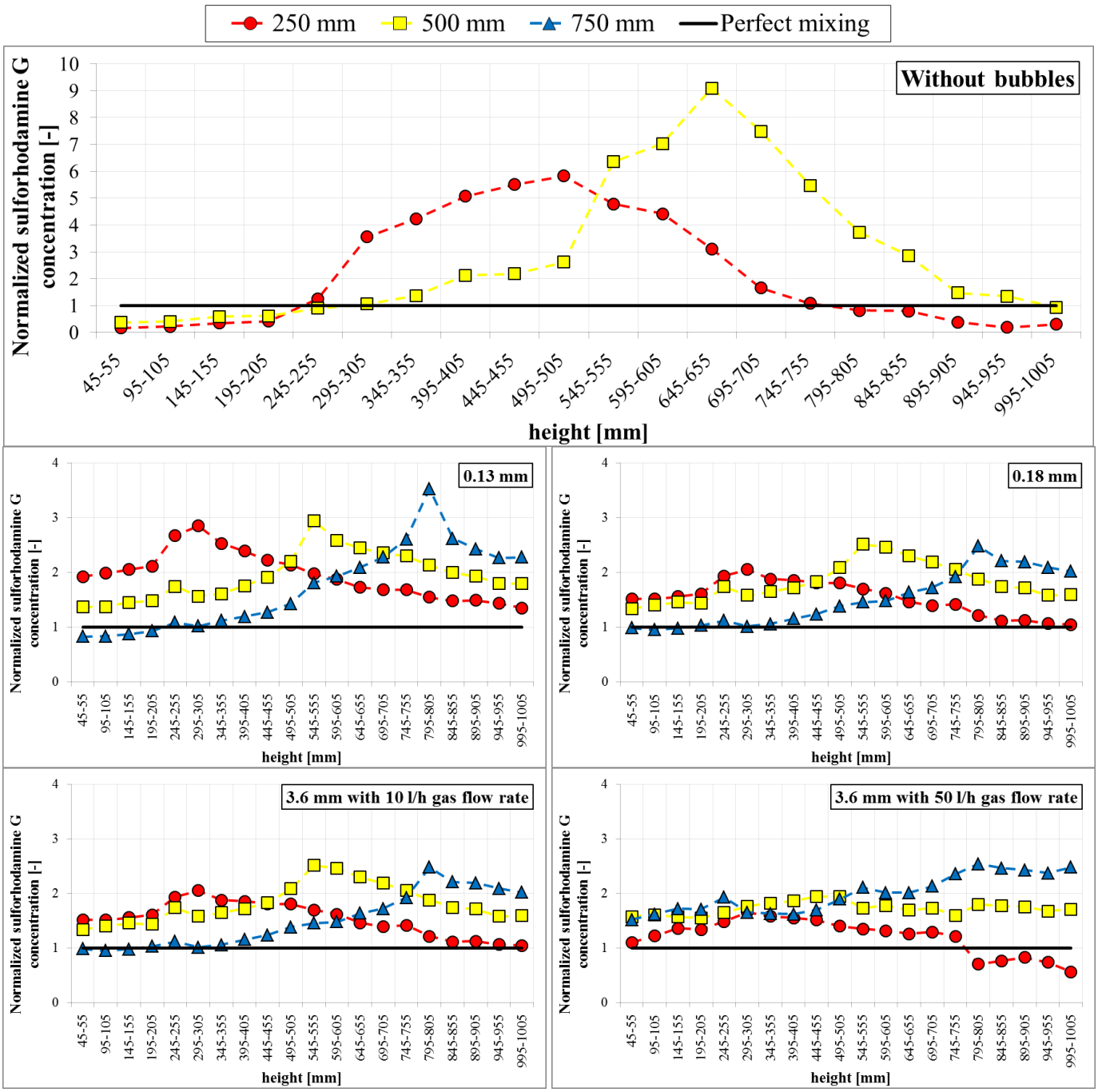

Figure. 9 Normalized dye concentration ratios at t=300 s without counter-current liquid flow in function of the column height. Dye inlets at 250, 500 and 750 mm, bubbles generated with 0.13, 0.18 and 3.6 mm capillaries.

5.2. Cases with counter-current liquid flow

The mixing performance was analysed in cases with counter-current liquid flow depending on the inlet position, capillary size (bubble size), and the counter-current liquid flow rate. Figure. 10 shows some exemplary snapshots from the measurements at t=300 s for different injection heights.

Compared to the stagnant case (Figure. 8, left image), where the dye just spread due to the inlet jet and stayed mostly above the inlet, this accumulation is hindered by the counter-current liquid flow and the dye is transported from the inlet to lower column regions in high concentrated pockets (Figure. 10, left image).

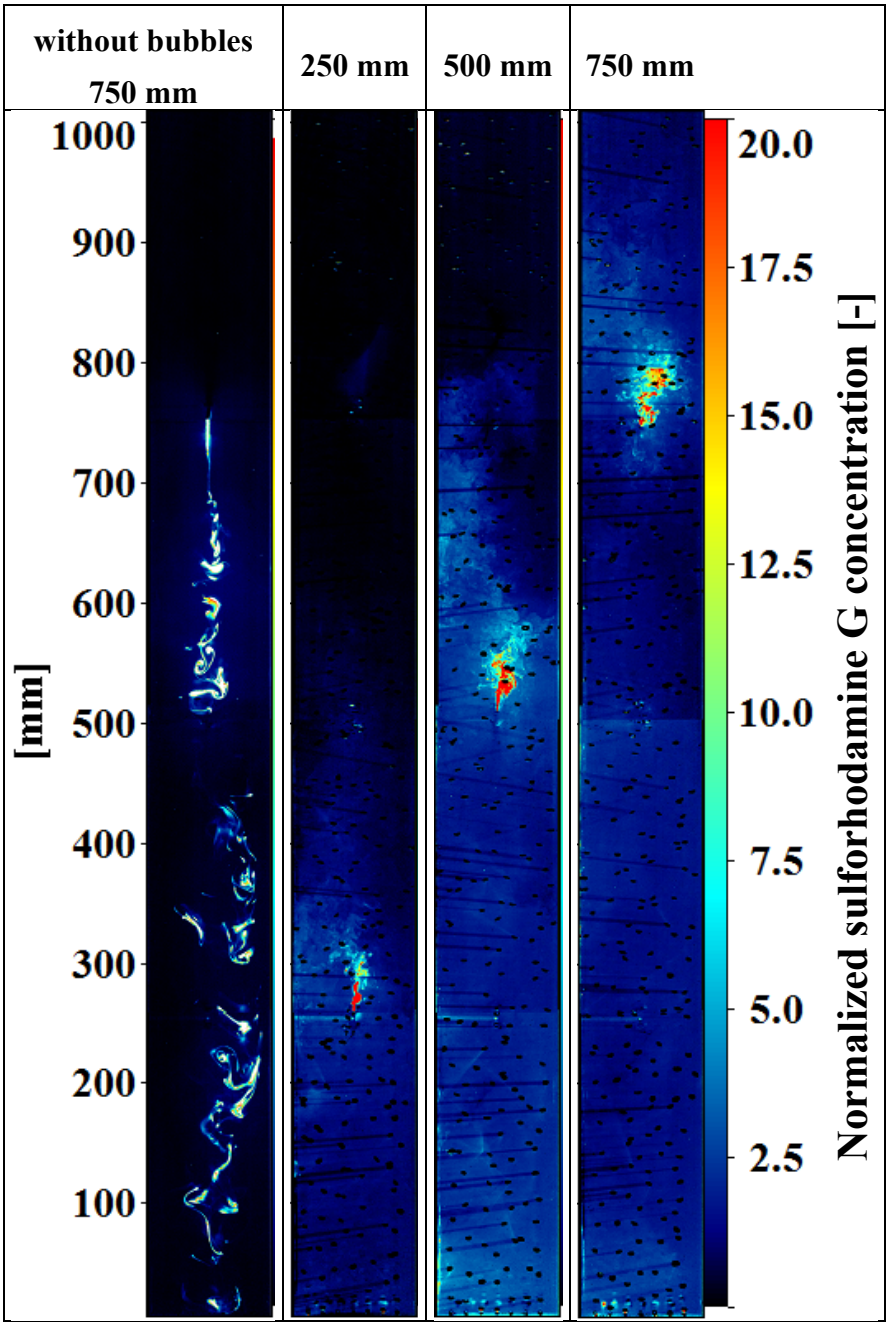

Figure. 10 Snapshots of the experiments with 11.1 l· min^{-1} counter-current liquid flow rate at t=300 s with and without bubbles. Dye inlet at 250, 500 and 750 mm, bubbles generated with 0.18 mm capillaries.

The bubbles, present in the right three cases shown in Figure. 10, induce an upward going flow that distributes the dye also slightly above the respective inlet positions. In the lower parts of the column a rather equal dye distribution at low concentration level exists, thus showing the homogenisation by bubble induced mixing.

In Figure 11 the normalized concentration ratios at 3.1 l· min^{-1} and 11.1 l· min^{-1} counter-current liquid flow rates are represented in function of the column height for the 0.18 mm capillaries and three different injection heights. These curves also show the aforementioned difference between the case without bubbles and with bubbles, where a more equal distribution of the dye is achieved. Additionally, the higher the counter-current liquid flow rate, the larger the amount of dye transported downwards in the column. Therefore, in presence of counter-current liquid flow, as expected, a higher dye inlet is beneficial for mixing, otherwise many of the injected species will be quickly lost through the outlet (Figure. 11).

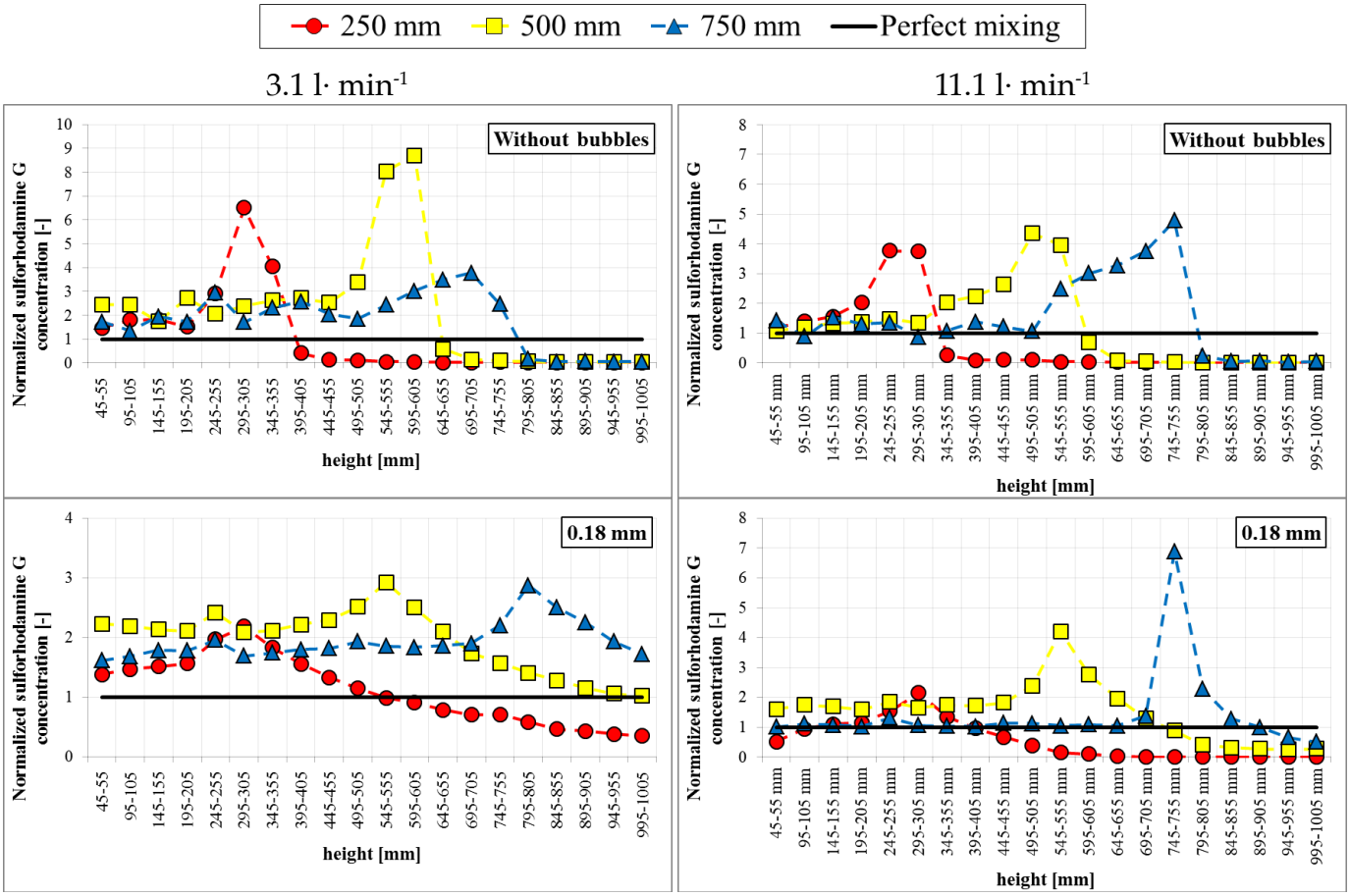

Figure. 11 Normalized dye concentration ratios at t=300 s with 3.1 l· min^{-1} and 11.1 l· min^{-1} counter-current liquid flow rates in function of the column height. Dye inlets at 250, 500 and 750 mm, bubbles generated with 0.18 mm capillaries.

The influence of the bubble size is shown on the snapshots of Figure. 12 at t=300 s for 3.1 l· min^{-1} counter-current liquid flow rates. The effective mixing induced by the bubbles can be seen once more in this figure. While the dye is distributed in packages by the counter-current flow for the case without bubbles on the left, the bubbly flow leads to an even distribution of the dye in the column.

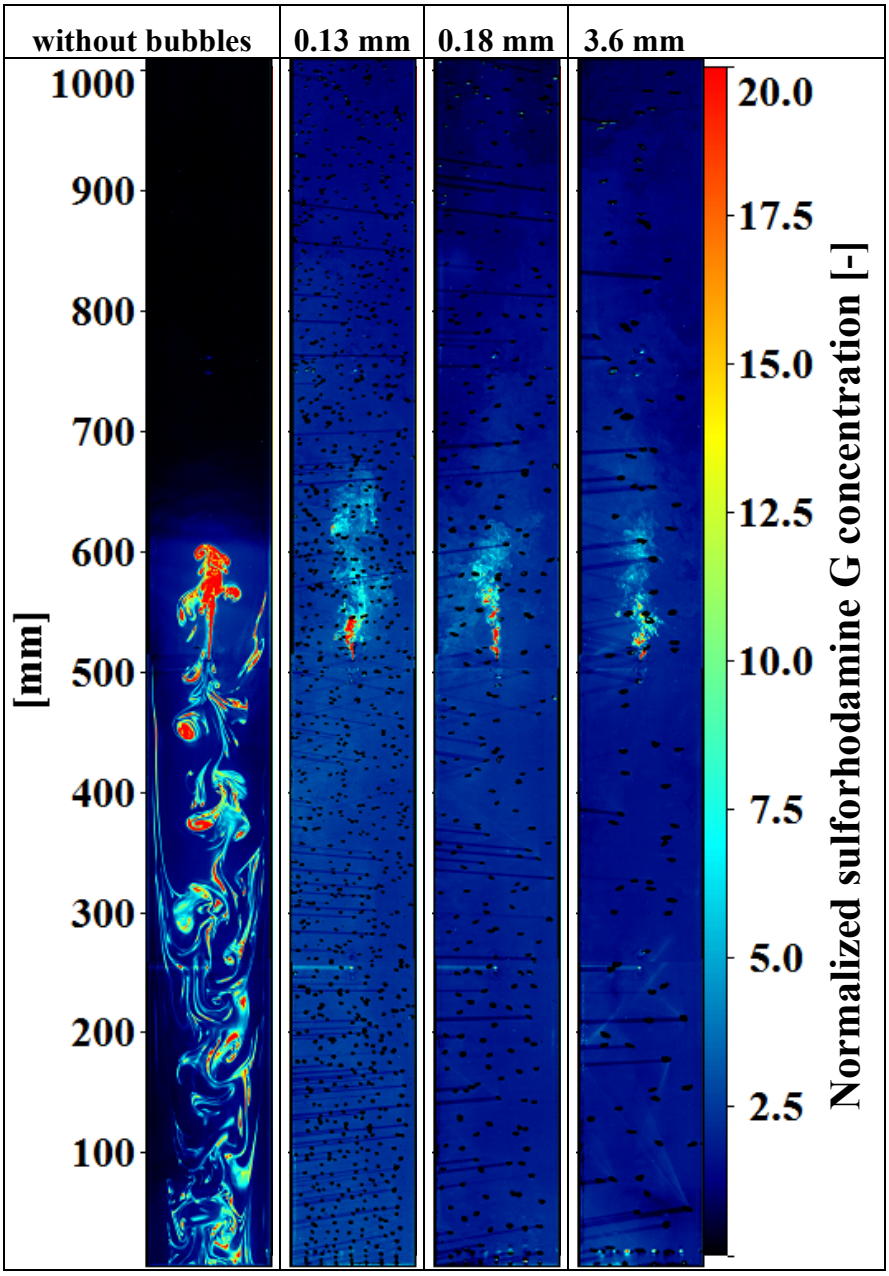

Figure. 12 Snapshots of the experiments with 3.1 l· min^{-1} counter-current liquid flow rate at t=300 s with and without bubbles. Dye inlet at 500 mm, bubbles generated with 0.13, 0.18 and 3.6 mm capillaries.

It is also noticeable that with increasing capillary diameter, thus bubble size, the inlet jet and its concentration values decrease, as well as the concentration in the whole measurement plane, which is related to a more efficient mixing of the whole column liquid content.

This decreasing trend of the concentration with increasing bubble size can also clearly be followed on Figure. 13, where the normalized concentration ratios are shown in function of the column height. As it was observed in the stagnant cases, not only an increasing capillary diameter, but also an increasing gas flow rate is also beneficial for mixing. The best mixing performance is found again with the largest capillary and at the highest gas flow rate.

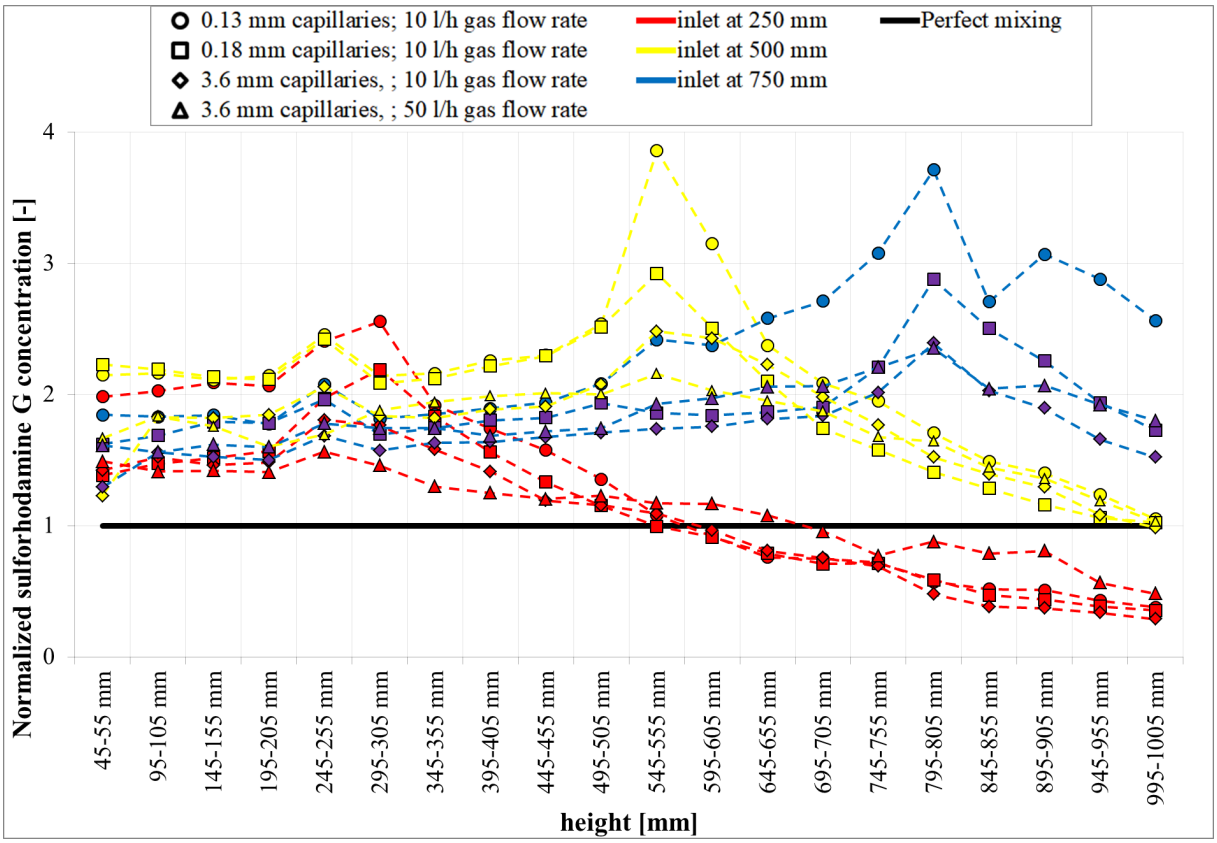

Figure. 13 Normalized dye concentration ratios at t=300 s for 3.1 l· min^{-1} counter-current liquid flow rate in function of the column height. Dye inlets at 250, 500 and 750 mm, bubbles generated with 0.13, 0.18 and 3.6 mm capillaries at 10 l· h^{-1} and 50 l· h^{-1} gas flow rate.

Finally, the influence of the counter-current liquid flow rate on the mixing efficiency is investigated. An exemplary result for the bubbly flow generated with the 0.18 mm capillaries at different counter-current flow rates is represented on Figure. 14, where the dye inlet was at 500 mm. At the two lowest counter-current flow rates the injected dye is almost equally distributed in the whole measurements plane, except from the inlet region, where much higher intensities can be observed. Although, at 3.1 l· min^{-1} the concentration at the top of the column

gets lower because at higher counter-current flow less dye is transported to the top of the column. With increasing counter-current flow rate the low concentration region above the dye inlet spreads. At 55.5 l· min^{-1} counter-current liquid flow rate it occupies the whole area above the inlet, all injected dye is forced to spread downwards.

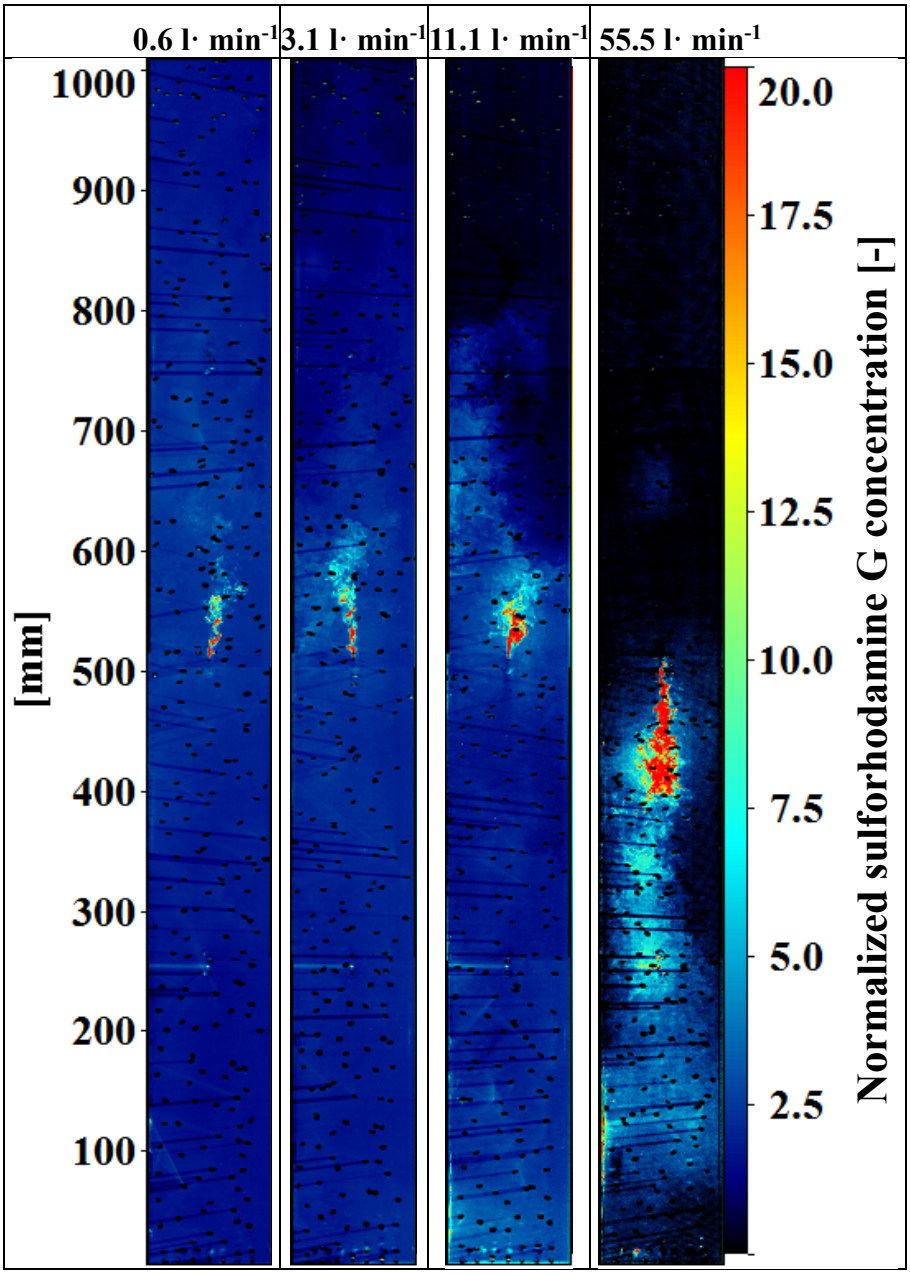

Figure. 14 Snapshots of the experiments with different counter-current liquid flow rates at t=300 s. Dye inlet at 500 mm, bubbles generated with 0.18 mm capillaries.

The average normalized concentration ratio results for these cases are depicted in Figure. 15 with yellow marks (middle image). The aforementioned mixing behaviour is also observed on these width averaged curves.

Also for the lower (red marks) and higher (blue marks) inlet positions the high peak concentration can be found just above the inlet position for 55.5 l· min^{-1} counter-current liquid flow rate. Here the bubbles are not able to disperse the injected high-concentrated dye due to the high counter-current liquid flow (the peaks are cut from the diagram due to scale issues). Below this peak, the normalized dye concentration decreases quickly and gets close to the perfect mixing condition, while above the inlet the concentration decreases to zero, because there, almost no dye exists. With decreasing counter-current liquid flow rate, the average dye concentration decreases for all inlet positions. It is also noticeable on these plots that with decreasing counter-current liquid flow rate more dye is transported in the upper column sections by the help of the bubble induced upward flow. Therefore, the measured concentration in the upper sections increases. As it was also observed on Figure. 14, the injected dye spreads almost equally above and below the dye inlet at the lowest two counter-current liquid flow rates. In the depicted case with 0.18 mm capillaries, best mixing was reached at 11.1 l· min^{-1} counter-current liquid flow rate.

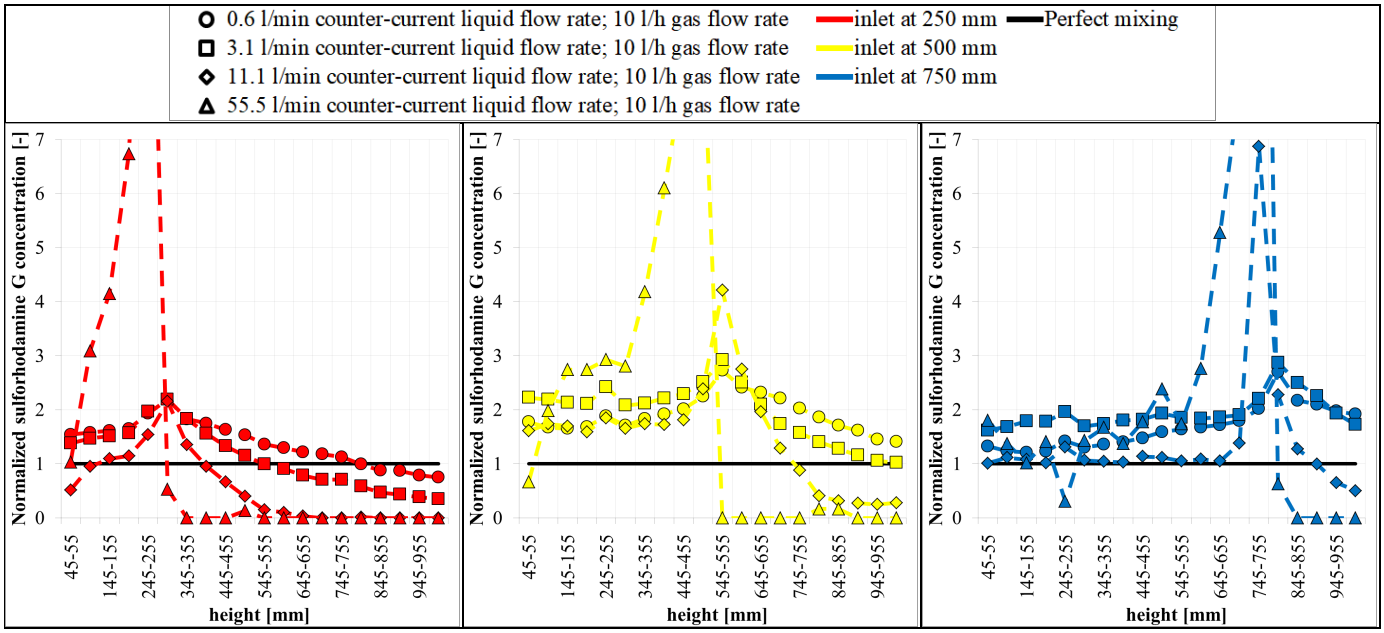

Figure. 15 Normalized dye concentration ratios at t=300 s for different counter-current liquid flow rates in function of the column height. Dye inlets at 250, 500 and 750 mm, bubbles generated with 0.18 capillaries (highest peaks are cut on the top for scaling reasons).

6. Conclusions

In this study bubble induced mixing in a bubble column has been examined by the help of tracer LIF measurements (Sulforhodamine G) combined with shadow imaging. Three different capillary diameters were used to generate bubbles in a wide diameter range of 1 to 9 mm. Also the gas and liquid flow rates have been varied in this study.

The strong influence of the bubbles presence, their size and the counter-current liquid flow rate on mixing in the column is obvious from these results. This influence is due to the significant differences of the bubble properties generated with the two smaller (0.13 and 0.18 mm) and with the large (3.6 mm) capillary, as well as the noticeable differences in bubble induced upward flow [Kováts and Zähringer, 2024]. These differences lead to the observed mixing behaviour, namely the larger the bubbles, the higher the bubble induced upward velocity, which leads to a better mixing.

The highest counter-current liquid flow rate led to a more concentrated dye jet, which was less dispersed than at lower liquid flow rates, while the moderate counter-current liquid flow rate (11.1 $l \cdot min^{-1}$) has been found optimal for mixing in the investigated cases. The combination of large bubbles generated with the 3.6 mm capillaries, and a moderate counter-current liquid flow rate led to the best mixing performance in the bubble column. In cases, where mass transfer from the gas to the liquid has to be considered, larger interfacial area, and therefore smaller bubbles are preferred. Then, a compromise has to be found to achieve sufficient mass transfer and mixing at the same time.

Acknowledgments

This work has been carried out in the frame of a joint research project (GZ: RZ 11/3-1 and ZA 527/3-1) funded by the German Research Foundation (DFG).

The authors would also like to acknowledge the help of their student Jianye Han in doing the experiments and parts of the postprocessing. The workshop of LSS is acknowledged for its help in mounting the experimental set-up.

References

Alméras, E., Cazin, S., Roig, V., Risso, F., Augier, F. and Plais, C. (2016). Time-resolved measurement of concentration fluctuations in a confined bubbly flow by LIF. *International Journal of Multiphase Flow*, 83, 153

Alméras, E., Plais, C., Roig, V., Risso, F. and Augier, F. (2018). Mixing mechanisms in a low-sheared inhomogeneous bubble column. *Chemical Engineering Science*, 186, 52-61

Bai, W., Deen, N. G. and Kuipers, J. A. M. (2012). Numerical Investigation of Gas Holdup and Phase Mixing in Bubble Column Reactors. *Industrial & Engineering Chemistry Research*, 51, 1949

Bothe, D., Shirzadi, H. and Warnecke, H.-J. (2007). Evaluations of Euler-Euler Simulations of Bubble Columns Based on Numerical Tracer Experiments. *Chemical Engineering Research and Design*, 11, 1491-1496

Bouche, E., Cazin, S., Roig, V. and Risso, F. (2013). Mixing in a swarm of bubbles rising in a confined cell measured by mean of PLIF with two different dyes. *Experiments in Fluids*, 54 (6), 1552

Ekambara, K. and Joshi, J. B. (2003). CFD Simulation of Residence Time Distribution and Mixing in Bubble Column Reactors. *Canadian Journal of Chemical Engineering*, 81, 669–676

Kováts, P. and Zähringer, K. (2024). Statistical Analysis of Bubble Parameters from a Model Bubble Column with and without Counter-Current Flow. *Fluids*, 9(6), 126 https://doi.org/10.3390/fluids9060126

Kováts, P., Velten, C., Mansour, M., Thévenin, D., Zähringer, K. (2020). Mixing characterization in different helically coiled configurations by laser-induced fluorescence. *Exp. Fluids 61*, 203, doi:10.1007/s00348-020-03035-0

Roudet, M., Billet, A. M., Cazin, S., Risso, F., & Roig, V. (2017). Experimental investigation of interfacial mass transfer mechanisms for a confined high-reynolds-number bubble rising in a thin gap. *AIChE Journal*, 63 (6), 2394-2408

Shetty, S. A., Kantak, M. V. and Kelkar, B. G. (1992). Gas-Phase Backmixing in Bubble-Column Reactors. *AIChE Journal*, 38, 1013-1026

Wiemann, D. and Mewes, D. (2005). Prediction of Backmixing and Mass Transfer in Bubble Columns Using a Multifluid Model. *Industrial & Engineering Chemistry Research*, 44, 4959-4967